THE
PHYSICAL
SOCIETY

MEMOIRS

OF THE

COLLEGE OF SCIENCE

KYOTO IMPERIAL UNIVERSITY

SERIES A

VOL. XII, No. 3

MAY 1929

KYOTO

A Sensitive Reaction of Cuprous Ion

By

Otozo Funakoshi

(Received April 11, 1929)

A short time ago F. Feigl[1] reported that p-dimethylaminobenzylidene rhodanine may serve as an extremely sensitive reagent for silver, with which the reagent forms a reddish violet precipitate. Just at that time as I was engaged in a work which necessitated my finding some means to precipitate cuprous copper from a solution as completely as possible, I naturally thought of the applicability of Feigl's reagent for this purpose, and tried to find out with what sensibility cuprous copper may thus be precipitated.

For reduction of copper, a saturated sodium bisulphite solution prepared by passing sulphur dioxide into a sodium carbonate solution till the solution gave a neutral reaction to litmus paper, was used. About 1.2 c.c. of such a solution was found to be quite sufficient completely to reduce 5 c.c. of 1% copper sulphate solution instantaneously.

As the reagent for silver precipitation, Feigl dissolved 0.03 gram of the rhodanine in 100 c.c. of acetone. In my case, however, it was inconvenient to use acetone solution, as this solvent forms with sodium bisulphite an insoluble addition-product so as to make the precipitation of the copper compound ambiguous. So an alcoholic solution containing 0.03 gram of the rhodanine in every 100 c.c. was taken, and this was added to the copper solution slightly in excess. Care must always be taken not to use the reagent in a large excess, otherwise the rhodanine separates out from the solution and contaminates the precipitate of copper. Whenever such contamination is suspected the solution in which copper rhodanine is suspended must be shaken with ether in order to dissolve the co-precipitated free rhodanine.

---

1. Zs. anal. Chem., **74**, 380 (1928)

To 5 c. c. of a copper solution containing 0.00127 gram of copper in the cuprous state, 18 c. c. of the alcoholic rhodanine solution above stated were added and the progress of the precipitation in a neutral solution was compared with that in a solution faintly acidified with sulphuric acid.

Neutral solution.	Acid solution.
A reddish violet precipitate was formed instantly and the solution became clear after an hour.	A reddish violet precipitate was formed instantly, but the solution did not become clear even after 2 hours.

Cupric ion also combines with the rhodanine and forms a brown precipitate in a neutral solution and yellowish green needle crystals in an acid solution. They are both soluble in water.

Neutral solution.	Acid solution.
The solution gradually became turbid and precipitated a brown substance. The solution coloured red, did not become clear unless left to stand for a long time.	The yellowish green crystals separated out. The solution was yellowish brown.

The precipitate of the cuprous compound is of reddish violet colour and resembles the corresponding silver compound very much. It is exceedingly insoluble in water, but as copper slowly undergoes oxidation to the cupric state it can not be washed with water repeatedly. When exposed in air for a few days the copper compound gradually decomposes and becomes dark brown.

In order to learn with what degree of accuracy the reaction may be employed for qualitative detection of copper, the sensibility of the reaction was examined by gradually increasing the dilution of the copper solution from which the metal was to be precipitated. The alcoholic solution of the precipitant was always used slightly in excess. The results are shown in the table given below.

The sensibility of the reaction by which copper in the cuprous state can be precipitated from a neutral solution with p-dimethylaminobenzylidene rhodanine is thus calculated to be 1 : 4,000,000. This is nearly of the same degree as the sensibility of silver precipitation, which was determined by Feigl[1] to be 1 : 5,000,000.

---

1. loc. cit.

Copper sulphate solution		Copper gm.	Sod. sulphite solution	Precipitant c.c.	Remarks
%	c.c.				
0.1	1	0.000254	3 drops	3.7	Immediate pption
0.01	1	0.0000254	2 „	1.0	„ „
0.0004	2	0.000002032	2 „	1.0	Pption after 10 minutes
0.0002	2	0.000001016	2 „	1.0	„ „ 30 „
0.00013	2	0.000000677	2 „	1.0	„ „ „ „
0.000125	2	0.000000635	2 „	1.0	„ „ 12 hours
0.0001	2	0.000000508	2 „	0.8	Ppte faintly observable after 12 hours

The writer takes this opportunity warmly to thank Professor Motooki Matsui under whose encouragement the work was carried out.

Crystal-Faces developed by etching Metallic Crystals of Aluminium and Zinc

By

Buntaro Fujita

(Received April 12, 1929)

Abstract

When the surface of a block of the single-crystal of a metal is etched by some reagent, its surface shines brightly in several directions. This seems to be caused by the reflection of light at many small and regularly arranged facets of the crystal, which are developed by etching. In the present experiment the writer has determined the crystallographic indices of the crystals of aluminium and zinc, by means of an optical goniometer and X-ray analysis. In the case of the aluminium crystal these facets are (100) and (110), the intensity of light reflected from the (110) facets being much fainter than that reflected from the (100) facets. In the case of the zinc crystalthese facets are (0001) and (10$\bar{1}$0).

The specimens of aluminium examined in the present experiment were taken from commercial wires of 3 mms. in diameter and commercial plates of 1–1.5 mms. in thickness, and the specimens of zinc were also taken from commercial plates of 1–1.5 mms. in thickness. To cause the crystal to grow, the method of straining followed by heat-treatment was applied.[1] When the surfaces of specimens thus prepared are etched by HCl, HF and NaOH etc., their surfaces shine brightly in several directions. This means that the etched surface is not a flat surface, but consists of many zig-zag facets of the crystal, which are arranged regularly.

Experiments to determine the crystallographic indices of such facets of the crystal of aluminium have already been made by J.Weerts[2], Y. Shimizu,[3]

1 H. Carpenter and F. Elam, Proc. Roy. Soc., **100**, 329 (1922)
2 J. Weerts, Z. S. f. techn. Physik, **9**, 126 (1928)
3 Y. Shimizu, Sci. Rep. Tôhoku Imp. Univ., **16**, 621 (1927)

H. H. Potter and W. Sucksmith[1] and others, from the angular relation between the directions of the normals to such facets, which were obtained by measuring the reflected directions of the light falling on the etched surface at a certain direction. But the results obtained by these authors are not concordant. Shimizu obtained (221) faces as such facets, Weerts (100), and Potter and Sucksmith two kinds of faces, (100) and (110). As to the zinc crystal, no such experiment has yet been attempted, so far as the writer is aware.

Now, in the present experiment the indices of the crystal-facets developed by etching were obtained by comparing the orientation of the normals of such facets with that of the crystallographic axes of the single-crystal. The former was determined by using an optical goniometer as shown diagramatically in Fig. 1, and the latter by treating the Laue-photograph taken with the specimen with the globe and the spherical scale devised by Prof. U. Yoshida.[2] X-ray analysis is of course necessary, because it may sometimes be erroneous to determine the indices of the crystal facets only from the angular relation between the directions of the normals to such crystal facets.

Fig. 1

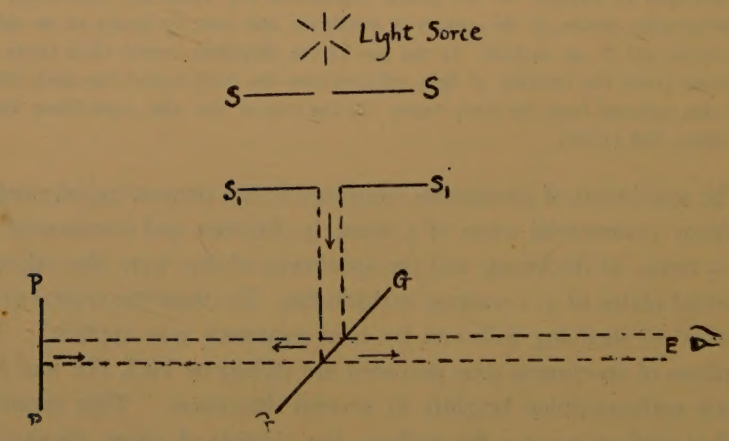

As the light source in the reflection experiment, an ordinary electric lamp is used. A bundle of parallel rays of about 1 cm.^{2} in cross-section limited by the two slits SS and S_1S_1 in Fig. 1, is first reflected by a glass

1 H.H. Potter and W. Sucksmith, Nature, **119**, 924 (1927)
2 U. Yoshida, Japanese, J. Phys., **4**, 133 (1927)

plate GG standing at 45° to the incident rays, and then it is sent to the surface of the specimen at PP. The position E of the observer is just opposite to the specimen in reference to the glass plate GG. If the specimen at PP is properly rotated about two axes, one horizontal and the other vertical, we can find several positions of the specimen at which the surface is most brilliant. In each one of such positions of the specimen the direction of both the incident and the reflected rays coincides with that of the normal to one of the crystal facets, and thus we can easily find the orientation of the normals to the crystal facets referring to the specimen; and consequently we can find the latitude Φ and the longitude Θ of the normals to the crystal facets referring to the surface of the specimen.

Practically the reflected light does not come suddenly to the observer brilliantly just at the position expected from the law of reflection, but it becomes brilliant gradually within a certain angular interval ($\pm 3°$) of the orientation of the specimen. These circumstances hinder the precise determination of the orientation of the crystal facets. This inaccuracy of the orientation of the crystal facets was made up for to some extent in the present experiment by taking the mean value of several different observations of the latitude and the longitude of the normal to the same crystal facet.

I. Aluminium Crystal

About thirty specimens were examined in the present experiment and in all cases the indices of the crystal faces developed by etching were (100) and (110), (for examples, see Table I). This means that the crystal faces developed by etching belong to one of the following two cases.

a. An assemblage of the cube-faces (100) and the dodecahedral faces (110). (Fig. 2a and Fig. 2b).

b. A combination of the dodecahedral faces and the cube-faces. (Fig. 3).

Table I

	Φ	Θ	Φ	Θ	Φ	Θ	Φ	Θ	Φ	Θ	Φ	Θ	Φ	Θ	Φ	Θ
By optical method	42°	26°	176°	57°	302°	20°	73°	62°	142°	19°	203°	18°	264°	55°	350°	30°
By X-ray analysis	40°	27°	180°	60°	300°	18°	72°	66°	142°	25°	207°	19°	268°	55°	348°	32°
Indices of the crystal faces	100		001		0$\bar{1}$0		101		011		$\bar{1}$01		0$\bar{1}$1		1$\bar{1}$0	

Fig.2a

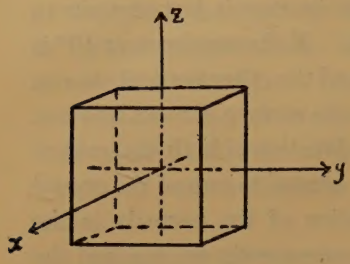

Fig.2b

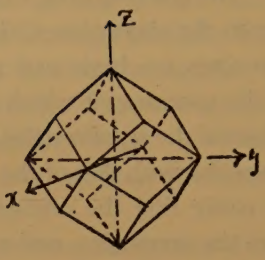

Fig.3

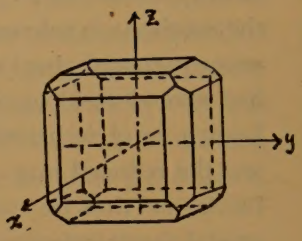

Of these two cases, the latter seems to be more probable than the former; because the intensity of the light reflected from the (110) faces is alway fainter than that from the (100) faces in a certain ratio. Thus considering, the case of Table I seems to be such as shown graphically in Fig.4, where the crystal faces developed by etching are a combination of cube and dodecahedron, the corners of the cube being truncated by the faces of the dodecahedron.

Fig.4

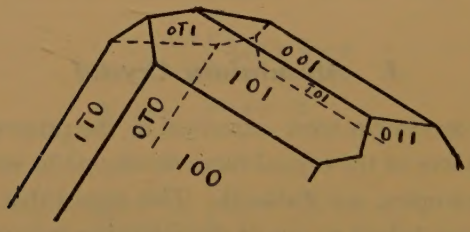

The results described above are independent of the kind and the concentration of the etching solutions so far as the present experiment is concerned. By using HCl, HF, and NaOH as etching solutions, and by changing their concentrations from 5% to 50% the writer obtained the same results as those stated before.

II. Zinc Crystal

By optical measurement on about ten single-crystal plates, the directions of the reflecting facets of the crystal were found to coincide with those of the crystal faces forming a hexagonal prism. Thus we can imagine two possible cases of the crystal faces developed by etching, the first consisting of the faces (0001) and ($10\bar{1}0$), and the second (0001) and ($11\bar{2}0$). To select the actual one from these two, we must know the orientation of the crystal-

lographic axes of the zinc crystal in reference to the specimen ; and this was done by taking a Laue-photograph. In such a manner, the indices of the crystal faces developed by etching the zinc crystal were ascertained to be (0001) and ($10\bar{1}0$) as shown in Fig. 5. The results of observation on one specimen are given in Table II as an example.

Table II

	Φ	Θ	Φ	Θ	Φ	Θ	Φ	Θ
By optical method	290°	45°	30°	8°	88°	42°	164°	32°
By X-ray analysis	290°	45°	30°	8°	85°	42°	160°	33°
Indices of the crystal faces	0001		$10\bar{1}0$		$01\bar{1}0$		$\bar{1}100$	

Fig.5

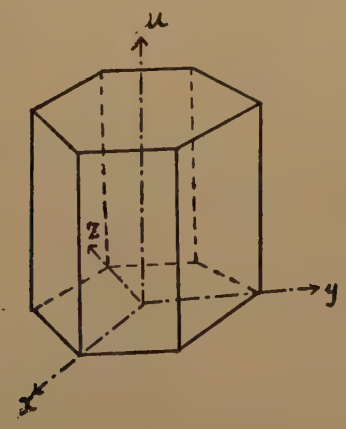

In conclusion, the writer wishes to express his sincere thanks to Prof. U. Yoshida for his kind guidance in the research.

Tensile Strength and Fracture of Rolled Strips of Molybdenum

By

Takeo Fujiwara

(Received April 20, 1929)

Abstract

The tensile strength of rolled strips of molybdenum, especially in reference to the direction of rolling, was tested by an ordinary tensile testing machine, and their fractures were examined by means of micro-photographs and X-rays.

The tensile strength is seen to differ according to the inclination of the direction of tension to that of the rolling. When the strip is cut thin along the direction of rolling, and the tension is applied in the lengthwise direction of the strip—that is, in the direction parallel to that of rolling—the tensile strength is seen to be greater by about 20% than when the inclination of the direction of tension to that of rolling is 45° and 90°.

Many strips are broken by applying the tension in various directions; and it is inferred, from the direction of the line of fracture, that the break occurs at the atomic planes (211) and (110) of the cubic crystal of molybdenum.

Introduction

In 1923 G. I. Taylor and C. F. Elam[1] studied the distortion of an aluminium crystal during a tensile test. In 1925 they[2] examined the plastic extension and fracture of an Al crystal. Recently tensile tests have been applied to alloy crystals of various metals by C. F. Elam.[3] C. H. Mathewson[4] investigated the plastic deformation of coarse-grained zinc, and he described also the phenomena obtained by stretching single crystals of Zn, with special reference to the direction of rolling in the parent strip and the direction of the slip band. According to Mathewson the manner of the

1 Taylor and Elam; Proc. Roy. Soc., **102**, 643 (1923)
2 Taylor and Elam; Proc. Roy. Soc., **108**, 28 (1925)
3 C. F. Elam; Proc. Roy. Soc., **109**, 143 (1925)
„ **115**, 133 (1927)
„ **116**, 694 (1927)
4 C. H. Mathewson; The A. Institute of M.M.E., No. 1623, (1927)

breaking caused by tension is different according as the tension is applied in the direction parallel to that of rolling or perpendicular to that direction. This point was examined by preparing specimens cut thin along the direction of rolling and along the direction perpendicular to it. In the former case two (or more) sets of twin bands occurred, and in the later case two different types of failures were found. The first type was due to a simple cleavage of the basal plane, and the second type was due to one set of parallel twin bands thickly covering the surface of the specimen.

In the present experiment the tensile strength of rolled strips of molybdenum, especially in reference to the direction of rolling, which was carried out at room temperature, and the manner of their fractures were examined.

Experimental Method and Results

A. The specimen

The specimen now examined was a rolled molybdenum plate which was 0.009 cms. in thickness, 8 cms. in width and 35 cms. in length. It was carefully rolled always in the same direction by the ordinary rolling process. The width of the strips examined was 0.55 cms, and their length varied from 7 to 13 cms. These strips were obtained from the rolled plate above stated by so cutting it in different directions that the lengthwise directions of the strips, that is the direction of the tension to be applied afterwards, made various angles with the direction of rolling ; the values of the angles given to various strips represent these angles.

B. Tensile strength

The tensile strength of these strips was measured by the usual testing method with an ordinary tensile testing machine. The tensile strengths, in k.g. per mm^2, obtained for various strips are tabulated in Table I, where the values for the strips 0°, 22.5°, 45°, 67.5° & 90° are given in the 2nd, 3rd, 4th, 5th and 6th columns respectively. The mean value for each group of the strips is given at the bottom of each column respectively.

From Table I it can easily be seen that the tensile strength of the rolled strip of molybdenum differs with the direction of the rolling. In the direction parallel to that of rolling it is maximum, and it is minimum in the directions making respectively angles of 45° and 90° with the direction of rolling.

C. Fracture of the broken strip

After the tensile strength was measured, photographs of the fractures of the tested specimens were taken from two different directions. First the

Table I

Tensile Strength of Molybdenum Strip in k.g. per mm^2

No. of Specimen	Strip 0°	Strip 22.5°	Strip 45°	Strip 67.5°	Strip 90°
1	109 5	106.5	88.8	105.1	80.8
2	114.5	98.8	96.2	91.6	84.6
3	118.8	101.0	93.5	95.1	95.6
4	99.5	102.2	97.6	100.2	95.8
5	108.8	109.9	91.5	100.3	99.2
6	120.0	77.5	97.5	96.0	95.5
7	114.2	105.2	98.8	101.1	93.0
8	120.0	108.2		91.4	97.1
9	113.1			100.4	93.5
10	118.8			97.1	
11	110.2			103.8	
12	118.9			82.3	
Mean Value	113.9	101.2	94.8	97.0	92.8

side view of the edge of the fracture was photographed, and then its end-on view was taken. The magnification of the former was about 13 and that of the latter was about 60.

Some of the photographs thus taken are reproduced in Figs. in Plates I and II, where Figs. 1, 2, 3, 4, and 5 of Plate I are the side view of the edges of the strips 0°, 22.5°, 45°, 67.5° and 90° respectively. Figs. 6 & 7 of Plate I and Figs. 1, 2 & 3 of Plate II are the end-on view of the strips 0°, 22.5°, 45°, 67.5° & 90° respectively.

The angle ϕ between the edge of the fracture and the direction of the tension applied, that is length-wise direction of the specimen, was measured for every specimen by the micro-photographs. The angle ε between the two sides forming the wedge of the fracture was also observed by the micro-photographs taken in the end-on direction of the wedge. These results are tabulated in Table II, where the No. of the specimen, which corresponds to that in Table I, is given in the 1st column, and the angle ϕ for the strips 0°, 22.5°, 45°, 67.5° and 90° is given in the 2nd, 4th, 6th, 8th and 10th columns respectively. The values of the angle ε are given in the 3rd, 5th, 7th, 9th

and 11th columns respectively. In the case of the fracture which is composed of several broken lines as shown schematically in Fig. 1, the angle ψ for each of these broken lines, such as a, b & c are tabulated; and when the value of ψ was greater than $\frac{\pi}{2}$ its supplement is given with negative sign, as shown in Fig. 1. The mean value for each group of the strips is given at the bottom of each column.

Fig. 1

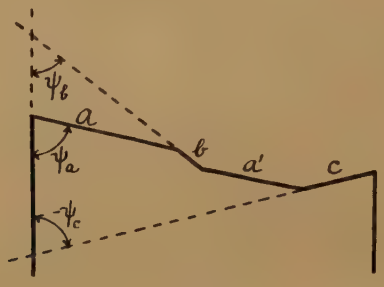

Table II

The Values of ψ and ϵ, in Degrees

No. of Specimen	Strip 0°		Strip 22.5°		Strip 45°		Strip 67.5°		Strip 90°	
	ψ	ϵ	ψ	ϵ	ψ	ϵ	ψ	ϵ	ψ	ϵ
1	68°, 45°	51°	57°	55°	60°	50°	68°	45°	90°	45°
2	66°,-85°	50°	59°	60°	58°	55°	68°	60°	90°	50°
3	70°,-74°	30°	58°	60°	58°	55°	69°	45°	90°	50°
4	78°,-50°	50°	58°	50°	47°	55°	70°	45°	90°	45°
5	70°, 47°	60°	50°	60°	55°	50°	69°	55°	90°	45°
6	66°, 84°	52°	58°	50°	60°	51°	71°	50°	90°	42°
7	66°,-85°	50°	67°	50°	70°	55°	66°	55°	90°	50°
8	70,°47°,-85°	30°	69°	55°			68°	45°	90°	50°
9	77°,-73°	50°					71°	45°	90°	47°
10	66°,-72°	50°					54°	45°	90°	50°
11							68°	50°		
Average	70,° 45,° and 75°	50°	58°	55°	60°	55°	68°	48°	90°	47°

From the photographs shown in Plates I and II, it can be seen that the edges of the fractures are nearly straight lines; and it was confirmed, from photographs taken of many specimens, that the angle ψ was nearly the same for different specimens belonging to the same kind of the strips. But, strictly speaking, the edge is not exactly straight, and it is composed rather of several broken lines. This tendency seems to be a little more marked in the cases of the strips 0°, 22.5° and 67.5° than in the others.

Lastly it was detected, from the enlarged photographs of the fractures, that the break down of the strips 0°, 22.5° and 45° was preceded by the slips of the crystals. This point was confirmed by projecting a parallel light on the slipped edge, and by detecting the presence of a great number of small metallic parallel planes there. In the cases of the strips 67.5° and 90°, especially in the latter, any trace of the slip of the crystal could scarcely be detected.

D. X-ray examination of the fracture

Next, the arrangement of the micro-crystals in some of the specimens was examined by means of the X-ray diffraction patterns which were taken at two different portions of the strip: one at the edge of the fracture, and the other at a portion about 2 mms. from the edge.

The method employed was just the same as in the case[1] of the rolled plates of tungsten and molybdenum. A Coolidge X-ray tube with molybdenum target was used, and the current passed through and the voltage applied were 10 milliamperes and about 40 K.V.s respectively. Generally the flat surface of the strip was set perpendicularly to the narrow beam of the X-rays. Some of the X-ray photographs thus taken are reproduced in Figs. 4, 5 and 6, Plate II.

Discussion of the Results

A. Arrangements of the micro-crystals in the rolled molybdenum strip and at the fracture

The arrangement of the micro-crystals in a rolled molybdenum strip has already been examined by the writer[2]. When the process of rolling advances always in the same direction, the micro-crystals are arranged in such a manner that one of the atomic planes (110), the diagonal plane, is arranged perpendicularly to the direction of rolling, and the atomic plane

---

1 T. Fujiwara; Mazda Kenkyu-Jiho **1**, No. 1, (1925)

2 *loc. cit.*

(100) which is perpendicular to the above mentioned diagonal plane is arranged nearly parallel to the surface of the strip. Strictly speaking, however, the orientation of the latter atomic plane is not exactly so for all the micro-crystals, but it takes the orientations rotated by various angles less than about ten degrees around the diagonal axis which is parallel to the direction of rolling.

Some of the photographs thus taken are shown in Plate II. Fig. 4 in Plate II is the diffraction pattern obtained with the original rolled strip. Figs. 5 and 6 in Plate II are those obtained at the edges of the fractures of the strips 0° and 90° respectively.

To make things clearer, the writer has sketched in Figs. 2 and 3, as the typical ones, the distribution of the radiating bands and the intense spots appearing in all the photographs taken. In these sketches the line OA represents the direction parallel to that of rolling on the photographic plate, the spots A′, B, C, D, E and F represent the intense spots, and the lines OA′, OB, OC, OD, OE and OF represent the radiating bands.

The sketch given in Fig. 2 represents the diffraction pattern obtained with the original rolled plate, and that given in Fig. 3 shows that obtained at the edges of the fractures of the strips 0°, 22.5° and 45°. By comparing the photographs, it was observed that the diffraction pattern obtained at the edges of the fracture with strips 67.5° and 90°, was nearly the same as that obtained with the original rolled plate; and that it was slightly modified with strips 0°, 22.5° and 45°, as shown in Fig. 3.

The only clear difference which we can recognize between Figs. 2 and

Fig.2

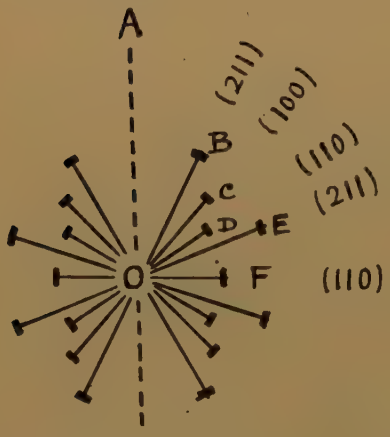

Fig.3

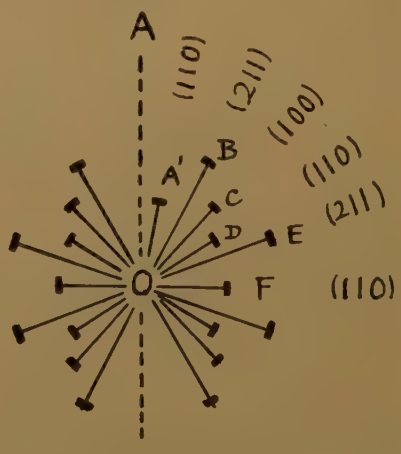

3, is that a new-radiating band OA′ due to the atomic plane (110) is added in Fig. 3 to the radiating bands shown in Fig. 2, in the direction making the angle of 10° to OA. This fact indicates that the micro-crystals at the edges of the fractures of strips 0°, 22.5° and 45° are so rearranged, by the fracture, that the atomic plane (110), which was previously perpendicular to the direction of rolling, now deviates from the former orientation by various angles less than about 10°. This is consistent with the occurrence of the preliminary slip of the crystals, at the fracture of strips 0°, 22.5° and 45°, previous to the rupture of the strips.

Fig. 4

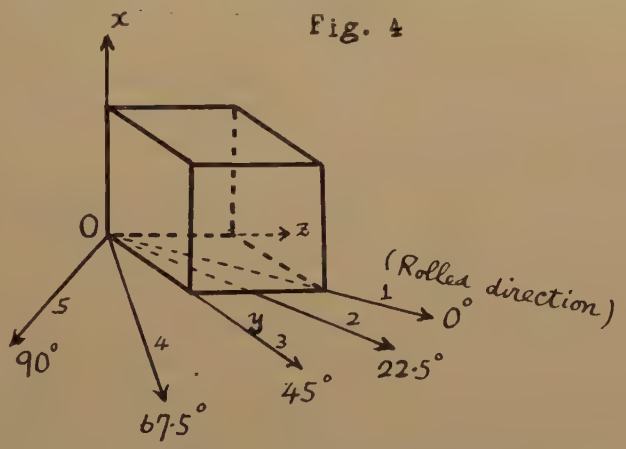

B. Fracture of the broken strips

As was stated before, the micro-crystals in a rolled strip of molybdenum are arranged nearly in the same orientation. Thus if we assume that the orientation of all of them is exactly the ideal one described before, then the direction of the tension applied to various kinds of the strips, in reference to the crystallographic axes, will be such as is represented in Fig.4. It is already known that the slip occurs along the atomic plane (110) or (211)[1] in the case of the tungsten crystal. Thus it seems not unnatural to suppose that the fracture, in our case, is caused by the slip along the atomic plane (110) or along the atomic plane (211). The orientation of the fracture plane will now be compared with that of the atomic plane (110) or (211), assuming that the direction of the tension applied is such as represented in Fig.4. From the values of ψ given in Table II, which is the angle between the edge of the fracture and the direction of the tension applied, the writer

1 Goucher; phil. Mag., **48**, 800 (1924)

calculated the values of the angle between the edge of the fracture and the diagonal line passing through the origin O of the square in the yz-plane in Fig. 4. This angle is represented by φ, and its values for various kinds of specimens are given in the third column of Table III. The values of ψ and ε in Table II are also included in the same table.

If the fracture of the specimen is caused by the slip along the atomic planes (110) and (211) as is assumed above, then the edge of the fracture must be the intersection of any one of these atomic planes with the rolled surface of the strip, that is the yz-plane in Fig. 4. The values of the angle between this intersection and the rolled direction, given in Table III, were calculated by picking out those which are very close to the values of φ for various kinds of strips; the indices of the atomic planes which are responsible respectively for each of these values of φ' are given in the 5th column of the same table. The agreement between the values of φ and φ' must be considered to be entirely satisfactory in this sort of experiment. Thus if our consideration be correct, that the fractures are caused by the slip along the atomic planes having the indices given in the fifth column of Table III, then the angles ε' between these atomic planes and the atomic plane (100), which is parallel to the rolled surface of the specimen, must be equal respectively to the values of ε given in the 4th column of Table III. In the 7th column of the same table, the calculated values of ε' for various atomic planes having the indices given in the 5th column are tabulated.

The atomic planes having the indices given in the 8th column are therefore selected so that the values of ε' are concordant respectively with

Table III

Kind of strip	ψ in degrees	φ in degrees	ε in degrees	Indices of the atomic plane	φ' in degrees	ε' in degrees	Indices of the atomic plane by which the fracture is caused
Strip 0°	70° 45° −75°	70° 45° −75°	50° 40° 50°	(121) (110) or (101) (112)	72° 45° −72°	53° 37° 53°	(121), (112), and (110) or (101)
Strip 22.5°	58°	35.5°	55°	(110)	45°	54°	(110)
Strip 45°	60°	15°	55°	(121)	18.5°	53°	(121)
Strip 67.5°	68°	0°	48°	(211) (011)	0° 0°	37° 90°	(211)
Strip 90°	90°	0°	47°	(211) (011)	0° 0°	40° 90°	(211)

those of ε, which must be regarded rather as rough estimations. Considering thus, it seems to be convincingly probable that the fracture of the specimens is caused by the slip along the atomic planes tabulated in the 8th column of Table III.

C. *Theoretical consideration*

When an external force is applied to a crystal and its value reaches a certain amount, the crystal is crushed into microcrystals and they tend to arrange themselves in a certain regular manner.

Now we consider the case of a single crystal which is subjected to a tension. If θ represents the angle between the direction of the tension applied and the normal to a possible slip-plane, η the angle between the projection of the direction of the tension on the slip-plane and a possible direction of the slip in the slip-plane, T the magnitude of the tension applied to the specimen, and A the area of the cross-section of the specimen in the direction perpendicular to that of the tension, then the component τ of the tension along the direction of the slip per unit area of the slip plane will be given by

$$\tau = \left(\frac{T}{A}\right)\cos\theta \sin\theta \cos\eta.$$

As was stated before, the micro-crystals in a rolled strip of molybdenum are arranged nearly in the same orientation, so that it may be regarded as being composed of a single crystal. Thus the writer assumed that the strip is composed of one block of a single crystal, and that the tension is applied to this single crystal in the directions shown in Fig. 4.

According to Goucher's study the slip occurs, in the case of tungsten, in the direction of [111] in the atomic plane (211). In the present case we have observed that the fracture is caused by the slip along some of the atomic planes (211) or (110). Next as to the direction of the slip in the slip planes (211) or (110), the writer examined the direction [111] and various other prominent crystallographic directions, but could not obtain any satisfactory result with any one of these axes. Consequently he disregarded entirely the slip direction, and assumed that the slip occurs with equal ease in all directions in the same slip plane. Thus he calculated the values of $\cos\theta \sin\theta$ for all the atomic planes (211) and (110), and they are given in the tables from IV to VIII. From these tables, the atomic planes which have comparatively large values of $\cos\theta \sin\theta$ are selected, and they are tabulated in Table IX.

Generally the atomic planes which have larger values of $\cos\theta \sin\theta$ are

less resistant against the extentional force; consequently if any extentional force be applied to the strip, the atomic planes which are tabulated in Table IX will slip easier than the others, and the strip will be broken along these atomic planes.

In Table IX, the kind of strips is given in the 1st column, comparatively large values of $\cos\theta \sin\theta$ in the 2nd column, and the indices of the atomic planes, to which those values of $\cos\theta \sin\theta$ are due respectively, are given in the 3rd column. The atomic planes whose indices are given in the 4th

Table IV, Strip 0°

Indices of the atomic plane	θ in degrees	$\cos\theta \sin\theta$
$(11\bar{2})$	−73.2°	−0.279
$(1\bar{2}1)$	−73.2°	−0.279
$(\bar{2}11)$	−54.5°	−0.473
$(12\bar{1})$	73.2°	0.279
$(1\bar{1}2)$	73.2°	0.279
(211)	54.5°	0.473
$(\bar{1}21)$	−30°	−0.433
(112)	30°	0.433
$(2\bar{1}1)$	90°	0
(121)	30°	0.433
$(\bar{1}12)$	−30°	−0.433
$(21\bar{1})$	90°	0
(011)	0°	0
$(01\bar{1})$	90°	0
(101)	60°	0.433
$(10\bar{1})$	−60°	−0.433
(110)	60°	0.433
$(1\bar{1}0)$	−60°	−0.433

Table V, Strip 22.5°

Indices of the atomic plane	θ in degrees	$\cos\theta \sin\theta$
$(11\bar{2})$	−86°	−0.070
$(1\bar{2}1)$	−53°	−0.481
$(\bar{2}11)$	−57°	−0.457
$(12\bar{1})$	53°	0.481
$(1\bar{1}2)$	−86°	−0.070
(211)	57°	0.457
$(\bar{1}21)$	−23.5°	−0.366
(112)	46.5°	0.500
$(2\bar{1}1)$	−77°	−0.219
(121)	23.5°	0.366
$(\bar{1}12)$	−46.5°	−0.500
$(21\bar{1})$	77°	0.219
(011)	24°	0.372
$(01\bar{1})$	66°	0.372
(101)	73°	0.280
$(10\bar{1})$	−73°	−0.280
(110)	48°	0.497
$(1\bar{1}0)$	−48°	−0.497

Table VI, Strip 45°

Indices of the atomic plane	θ in degrees	cosθ sinθ
$(11\bar{2})$	66°	0.372
$(1\bar{2}1)$	−35°	-0.470
$(\bar{2}11)$	−66°	−0.372
$(12\bar{1})$	35°	0.470
$(1\bar{1}2)$	−66°	−0.372
(211)	66°	0.372
$(\bar{1}21)$	−35°	−0.470
(112)	66°	0.372
$(2\bar{1}1)$	−66°	−0.372
(121)	35°	0.470
$(\bar{1}12)$	−66°	−0.372
$(21\bar{1})$	66°	0.372
(011)	45°	0.500
$(01\bar{1})$	45°	0.500
(101)	90°	0
$(10\bar{1})$	90°	0
(110)	45°	0.500
$(1\bar{1}0)$	−45°	−0.500

Table VII, Strip 67.5°

Indices of the atomic plane	θ in degrees	cosθ sinθ
$(11\bar{2})$	46.5°	0.500
$(1\bar{2}1)$	−23.5°	−0.366
$(\bar{2}11)$	−77	-0.219
$(12\bar{1})$	23.5°	0.366
$(1\bar{1}2)$	−46.5°	−0.500
(211)	77°	0.219
$(\bar{1}21)$	−53°	−0.481
(112)	86°	0.070
$(2\bar{1}1)$	−57°	−0.457
(121)	53°	0.481
$(\bar{1}12)$	86°	0.070
$(21\bar{1})$	57°	0.457
(011)	66°	0.372
$(01\bar{1})$	24°	0.372
(101)	73°	0.280
$(10\bar{1})$	73°	0.280
(110)	48°	0.497
$(1\bar{1}0)$	−48°	−0.497

Table VIII, Strip 90°

Indices of the atomic plane	θ in degrees	$\cos\vartheta \sin\vartheta$
$(11\bar{2})$	30°	0.433
$(1\bar{2}1)$	−30°	−0.433
$(\bar{2}11)$	90°	0
$(12\bar{1})$	30°	0.433
$(1\bar{1}2)$	−30°	−0.433
(211)	90°	0
$(\bar{1}21)$	−73.2°	−0.279
(112)	−73.2°	−0.279
$(2\bar{1}1)$	−54.5°	−0.473
(121)	73.2°	0.279
$(\bar{1}12)$	73.2°	0.279
$(21\bar{1})$	54.5°	0.473
(011)	90°	0
$(01\bar{1})$	0°	0
$(10\bar{1})$	−60°	−0.433
(101)	60°	0.433
(110)	60°	0.433
$(1\bar{1}0)$	−60°	−0.433

column, are those obtained by the observation of the fractures, and which are already given in Table III. If the atomic planes under consideration have the same absolute value of $\cos\theta \sin\theta$ in Tables IV,V,VI,VII and VIII, the plane which has a positive sign is tabulated in Table IX.

Table IX

Kind of strip	The value of $\cos\theta \sin\theta$	Indices of the atomic plane	Indices of the atomic plane obtained by micro-photos.
Strip 0°	0.473 0.433 0.433	(211) (121) & (112) (110) & (101)	(121) and (110)
Strip 22.5°	0.500 0.481 0.457 0.497	(112) $(12\bar{1})$ (211) (110)	(110)
Strip 45°	0.470 0.500	$(12\bar{1})$ (110) & (011)	$(12\bar{1})$
Strip 67.5°	0.500 0.481 0.457 0.497	$(11\bar{2})$ (121) $(21\bar{1})$ (110)	$(21\bar{1})$
Strip 90°	0.473 0.433 0.433	$(21\bar{1})$ $(11\bar{2})$ & $(12\bar{1})$ (101) & (110)	$(21\bar{1})$

From Table IX, we can see that, though the atomic plane which has the largest value of $\cos\theta \sin\theta$ among the atomic planes belonging to every kind of strip is not always the fracture plane observed by the micro-photographs, but the fracture planes observed by the micro-photographs have always comparatively large values of $\cos\theta \sin\theta$. Thus we may conclude that the fracture occurred along the atomic planes given in the last column of Table IX because they have comparatively large values of $\cos\theta \sin\theta$. A small discrepancy between the observation and the calculation, as seen in Table IX, must of course be allowed for in this sort of experiment, because the scattering of the orientation of the micro-crystals, and the other factors such as the simultaneous slippings along two atomic planes etc. are entirely ignored in the above calculation.

D. Tensile strength of the strip

As was stated in the preceding paragraph, the extentional force which will be needed to break the crystal is inversely proportional to $\cos\theta \sin\theta$, that is the tensile strength of the strip will depend upon the reciprocal of the value of $\cos\theta \sin\theta$.

Now from the results shown in Table IX the writer calculated the ratio of the value of $\cos\theta \sin\theta$ of strip 22.5° to that of strip 0°, and also the ratios of the values of strips 67.5° and 90° to that of strip 45°. The ratios thus obtained are expressed in percentage in the 6th column in Table X, where the kind of strip is given in the 1st column, the indices of the atomic plane along which the slip is occurred in the 2nd column, the value of $\cos\theta \sin\theta$ in the 3rd, and its reciprocal in the 4th column respectively. The tensile strength shown in Table I is reproduced in the 5th column, and the ratio of the values of the tensile strength corresponding to the ratio of $\cos\theta \sin\theta$ is given in the 7th column of the same table. In the case of strips 45°, 67.5° and 90° the slip-plane is (211), while in the case of strips 0° and 22.5° it is different. This is the reason why the ratios of the tensile strengths and of the values of $\cos\theta \sin\theta$ are taken separately in two cases.

It can be clearly seen that the ratios of the values of $\cos\theta \sin\theta$, agree well with those of the tensile strength, thus we can say reversely that the variation in the tensile strength of the rolled strips of molybdenum with reference to the direction of rolling is due to the arrangement of the micro-crystals in the rolled strip. Moreover the fine agreement between the calculation and the observation supports also reversely the considerations assumed in the preceding paragraphs.

Table X

Kind of specimen	Indices of the atomic plane	$\cos\theta \sin\theta$	$\frac{1}{\cos\theta \sin\theta}$	T. S.	Ratio in %	
					$1/(\cos\theta \sin\theta)$	T. S.
0°	(121) or (110)	0.433	2.31	113.9	100	100
22.5°	(110)	0.497	2.01	101.2	87.4	89
45°	(121)	0.470	2.13	94.8	100	100
67.5°	(211)	0.457	2.19	97.0	103	102
90°	(211)	0.473	2.11	92.8	99.1	98.0

In conclusion, the writer wishes to express his sincere thanks to Professor U. Yoshida, of Kyoto Imperial University for his invaluable suggestions.

Research Laboratory,
Tokyo Electric Company,
Kawasaki, Kanagawa-Ken,
Japan

Plate I

Fig.1, Strip 0°

Fig.2, Strip 22.5°

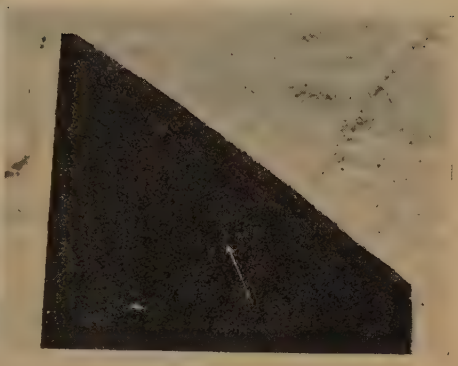

Fig.3, Strip 45°

Fig.4, Strip 67.5°

Fig.5, Strip 90°

Fig.6, Strip 0°

Fig.7, Strip 22.5°

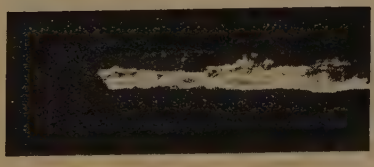

Plate II

Fig.1, Strip 45°

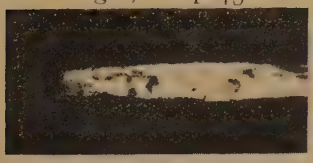

Fig.2, Strip 67.5°

Fig.3, Strip 90°

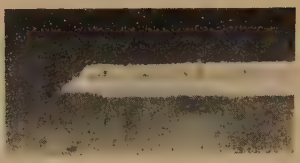

X-Ray Photographs of the Strip

Fig.4,
Strip 0° (original)

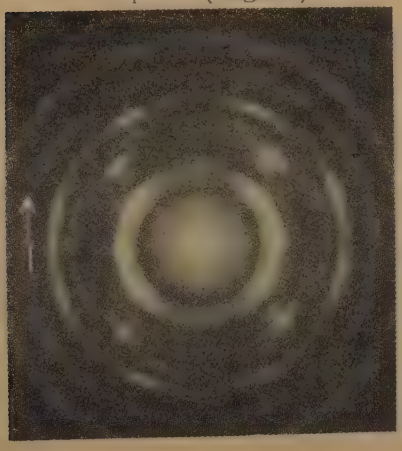

Fig.5,
Strip 0° (tested)

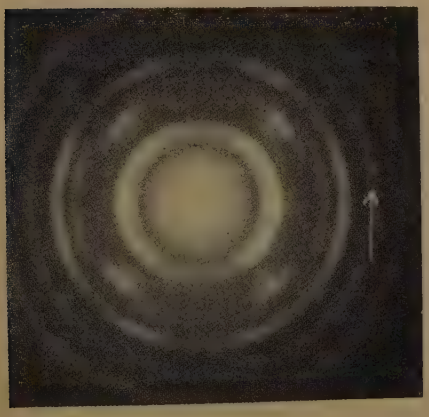

Fig.6,
Strip 90° (tested)

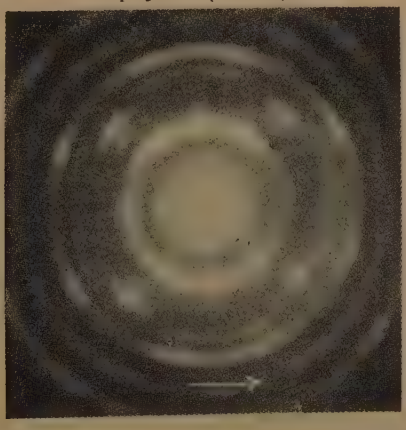

On the Effect of mixing Small Quantities of Cobalt with Brass

By

Daidzi Iitsuka

(Received April 26, 1929)

The present work has been undertaken with the object of finding out the effect of small quantities of cobalt when mixed with brass. It resulted in establishing the ternary equilibrium diagram in a corner, where the copper predominates in the ratio of 50%–100%, while zinc appears in the proportion of 0%–50% and cobalt, 0%–10%. Furthermore, some mechanical and corrosion tests were tried with a few new alloys which were considered technically important.

I The binary systems: Cu–Zn, Zn–Co and Cu–Co

For the Cu–Zn system, the author's own diagram[1] (Fig. 1), and for the Zn–Co system, Lewkonja's[2] (Fig. 2) were adopted not modified in any way. For the Cu–Co system, however, Sahmen's diagram[3] (Fig. 3) has to be modified, in so far as it concerns the curves for the primary crystallisation.

According to the author's experiment, copper and cobalt are not completely soluble in the molten state but form two liquid layers, the solubility-limits at a temperature a little higher than 1110°C being 3.5% Co on the copper side (=solution *d*) and probably 8% Cu on the cobalt side (=solution *b*). A series of cobalt-solid solutions separates out from the solution *d* on cooling till it goes into a peritectic reaction with the copper-rich melt at 1110°C. On cooling further, a series of copper-solid solutions is again forced

---

1 These Memoirs, A, **8**, 179 (1925)

2 Zs. f. anorg. Chem., **59**, 1 (1908)

3 *ibid.*, **57**, 293 (1907)

Fig. 1

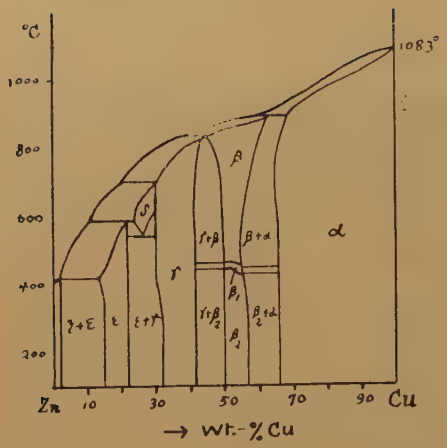

Fig. 2

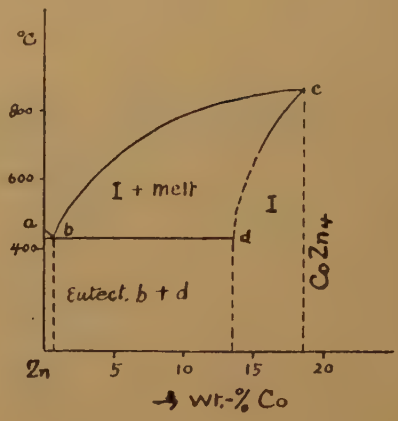

Fig. 3

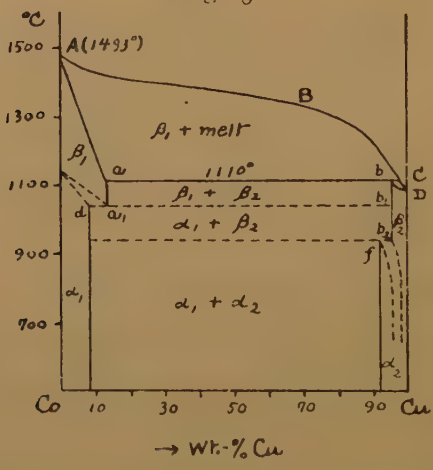

to crystallise till it reaches at last the copper-axis. According to Sahmen, this solid solution β_2 is destined to be transformed into α_2: such was however not found to be the case in the author's experiment. Fig. 4 is plotted mainly according to the author's own data, except that the details at the cobalt side are provisionally given in dotted lines, owing to the fact that the determinations with respect to those points are practically impossible.

II The ternary system: Cu–Zn–Co

An investigation of the ternary system Cu–Zn–Co within the narrow limit of 0.5%–5.0% Co to brasses with 70%, 60% and 55% Cu was attempt-

Fig. 4

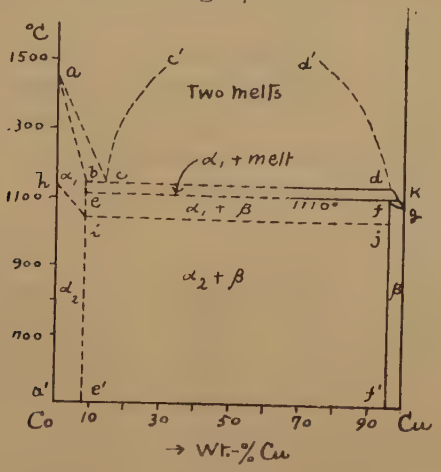

ed by Guillet[1] in 1920. The purpose of his investigation was not, however, to establish the ternary equilibrium diagram, but to find out the effect of cobalt on the mechanical properties and the microstructures of brass, and he concluded that cobalt has no favourable effect.

The present author, however, went on further in the limits of the composition, applied such means of investigation as thermal analysis, heat-treatments and microstructures, thereby being enabled to establish a part of the equilibrium diagram, and also to get a result differing from Guillet's in that the addition of some cobalt was found to be rather commendable in many cases.

Results of thermal analysis (Table III–X), heat-treatments and microstructures (Table XI), mechanical (Table XII) and corrosion tests (Table XIII) are each afterwards given in appropriate places.

The zinc and cobalt used as materials were both Kahlbaum's "pure" and the copper electrolytic. Changes of composition by volatilisation and oxidation were prevented as much as possible in this way, that the zinc was fused under molten sodium chloride in a porcelain crucible and kept slightly lower than its boiling point, and into it the copper and cobalt were alternately thrown in small pieces all the while being well stirred; thereupon the temperature was raised as much as would cause the mixture to come to a homogeneous solution. Furthermore, some of the alloys thus prepared, which are especially of technical importance, were analysed, the results of which

1 Rev. de Métallurgie, **17**, 494 (1920)

are given in Tables I and XII, inasmuch as the data given in Table II refer simply to the numbers of the mixed quantities.

On the basis of those data, the ternary equilibrium diagram, Fig. 5, was constructed, and its projection is shown in Fig. 6. The dotted lines there refer to the field boundaries at higher temperatures, while the full lines refer to those at ordinary ones. The projective diagram is divided into the following nine fields for the sake of illustration :—

1. $a'b'h'p'jk'a'$, 2. $b'c'h'b'$, 3. $e'c'h'f$,
4. $fh'p'g$, 5. $gp'n'i$, 6. $in'u'lq$,
7. $p'js'm'olu'n'p'$, 8. $x'lor'$, 9. qlx'.

Table I

No.	Cu %	Zn %	Co (diff.) %
119	99.14	0	0.86
115	95.17	0	4.83
107	81.04	0	18.96
13	91.07	7.73	1.20
15	89.43	7.77	2.80
16	88.09	8.14	3.77
105	70.26	9.69	20.05
68	74.89	24.61	0.50
71	74.03	24.39	1.58
61	72.18	24.88	2.94
88	63.72	29.18	7.10
33	62.12	35.69	2.19
101	57.08	35.72	7.20
90	50.74	29.71	19.55
74	51.97	45.37	2.66
25	57.01	41.43	1.56
26	51.21	44.88	3.91
111	51.84	45.69	2.47

Table II

No.	Cu %	Zn %	Co %
121	100	0	0
118	98	0	2
117	97	0	3
1	97	2	1
2	96	2	2
3	95	2	3
8	93	5	2
9	92	5	3
14	90	8	2
54	88	11	1
19	87	11	2

Table II continued

No.	Cu %	Zn %	Co %
76	84.5	15	0.5
77	84	15	1
78	83	15	2
79	82	15	3
92	79	18	3
67	79.5	20	0.5
64	79	20	1
65	77	20	3
102	75	23	2
63	74	25	1
69	71.5	28	0.5
47	71	28	1
46	70	28	2
70	69.5	30	0.5
53	69	30	1
43	68	30	2
48	67	32	1
40	66	32	2
116	96	0	4
120	90	0	10
4	94	2	4
5	93	2	5
99	92	2	6
6	90	2	8
7	85	2	13
98	91	5	4
10	90	5	5
97	89	5	6
11	88	5	7
12	85	5	10
96	87	8	5
17	86	8	6
18	82	8	10
20	85	11	4
94	84	11	5
21	83	11	6
22	81	11	8
23	79	11	10
103	83	13	4

Table II continued

No.	Cu %	Zn %	Co %
93	82	13	5
80	80	15	5
91	77	18	5
66	75	20	5
82	72	20	8
83	70	20	10
106	60	20	20
95	74	23	3
60	71	25	4
62	69	25	6
84	67	25	8
55	69	28	3
81	64	25	11
56	67	28	5
57	66	28	6
85	64	28	8
44	66	30	4
45	64	30	6
89	60	30	10
41	64	32	4
42	62	32	6
87	60	32	8
37	62	34	4
38	60	34	6
39	58	34	8
86	56	34	10
34	60	36	4
35	58	36	6
31	58	38	4
104	57	38	5
32	56	38	6
28	56	40	4
113	55	40	5
29	54	40	6
114	54	41	5
49	65	34	1
36	64	34	2
50	63	36	1
51	61	38	1

Table II continued

No.	Cu %	Zn %	Co %
30	60	38	2
52	59	40	1
27	58	40	2
58	56	41	3
72	57·5	42	0.5
59	57	42	1
24	54	45	1
109	51	45	4
73	54·5	45	0.5
112	50	46	4
110	51	47	2
75	54	42	4
108	53	42	5

Table III

No.	Liquidus °C	Solidus °C	Peritectic		Field & Structure
			°C	Sec.	
121	1083 (m.p. of Cu)				
119	1093	1087	—	—	
118	?	?	1108	1	
117	?	?	1108	5	
1	1091	1084	—	—	
2	?	1088	1103	4	
3	?	1093	1101	4	
8	?	1076	1096	?	
9	?	1088	1097	2	
13	1079	1054	—	—	
14	?	1062	1088	3	
15	?	1066	1090	4	
54	1068	1035	—	—	
19	?	1052	1072	5	
76	1045	1006	—	—	
77	1050	1008	—	—	
78	?	1010	1055	?	
79	?	1016	1055	3	
92	?	1005	1035	2	
67	1007	973	—	—	

a'b'c'h'p'jk'a'—field. (α)

Table III continued

No.	Liquidus °C	Solidus °C	Peritectic		Field & Structure
			°C	Sec.	
64	1017	977	—	—	a'b'c'h'p'j'k'a'—field. (s)
65	?	980	1029	?	
102	?	957	1005	?	
68	968	934	—	—	
63	970	940	—	—	
71	?	947	998	?	
69	955	915	—	—	
47	973	918	—	—	
46	975	922	—	—	
70	953	905	—	—	
53	955	910	—	—	
43	965	920	—	—	
48	950	—	917	2	
40	956	—	923	?	

Table IV

No.	Peritectic		Field & Structure
	°C	Sec.	
116	1108	7	e'd'c'h'f'—field. (α+γ)
115	1110	5	
120	1109	3	
107	1110	2	
4	1100	3	
5	1102	4	
99	1100	?	
6	1103	?	
7	1101	?	
98	1095	3	
10	1095	3	
97	1095	2	
11	1095	2	
12	1096	2	
16	1090	4	
96	1090	3	
17	1090	3	
18	1092	?	

Table IV continued

No.	Peritectic		Field & Structure
	°C	Sec.	
105	1068	?	e'd'c'h'f—field. ($\alpha+\gamma$)
20	1070	4	
94	1070	2	
21	1070	?	
22	1072	?	
23	1070	?	
103	1063	2	
93	1062	?	
80	1053	4	
91	1032	3	
66	1025	3	
82	1022	3	
83	1017	?	
106	1007	2	
95	1008	3	
61	1003	5	
60	1002	3	
62	1000	2	
84	998	?	
81	984	?	
55	985	?	

Table V

No.	Liquidus (α) °C	Solidus (α) °C	Field & Structure
56	979	948	f'h'p'g—field. ($\alpha+\gamma$)
57	978	943	
85	977	940	
44	975	940	
45	973	935	
88	972	930	
89	970	928	
41	970	927	
42	967	924	

Table VI

No.	Liquidus (α) °C	Peritectic °C	Peritectic Sec.	Field & Structure
87	970	927	3	gp'n'i—field. (α+β+γ)
37	968	927	3	
38	963	928	3	
39	960	926	4	
86	958	927	7	
34	956	927	4	
35	951	928	5	
101	948	927	9	
31	945	928	9	
104	943	926	10	
32	940	927	10	
28	934	928	10	
113	932	927	10	
29	930	927	6	
90	965	927	6	

Table VII

No.	Liquidus (β) °C	Solidus (β) °C	Liquidus (α) °C	Peritectic °C	Peritectic Sec.	Field & Structure
114	—	—	930	927	8	in'u'lq—field. (α+β+γ)
75	927	918	—	—	—	
108	928	919	—	—	—	

Table VIII

No.	Liquidus (α) °C	Peritectic °C	Peritectic Sec.	Solidus (β) °C	Liquidus (β) C°	Field & Structure
49	945	915	4	—	—	p'js'm'olu'n'p'—field. (α+β)
36	953	922	3	—	—	
50	938	917	7	—	—	
33	945	923	6	—	—	
51	928	918	10	—	—	
30	937	923	8	—	—	
52	924	918	7	909	—	
27	925	922	2	915	—	
58	929	925	2	?	—	
72	910	907	4	897	—	
59	919	917	7	906	—	
74	920	918	4	912	—	
24	—	—	—	888	913	
25	—	—	—	893	916	

Table IX

No.	Liquidus °C	Solidus °C	Field & Structure
73	900	885	x'lor'—field. (β)
111	908	895	
110	905	883	

Table X

No.	Liquidus (β) °C	Solidus (β) °C	Field & Structure
109	918	900	qlx'—field. (α + β)
26	922	913	
112	910	890	

Fig. 5

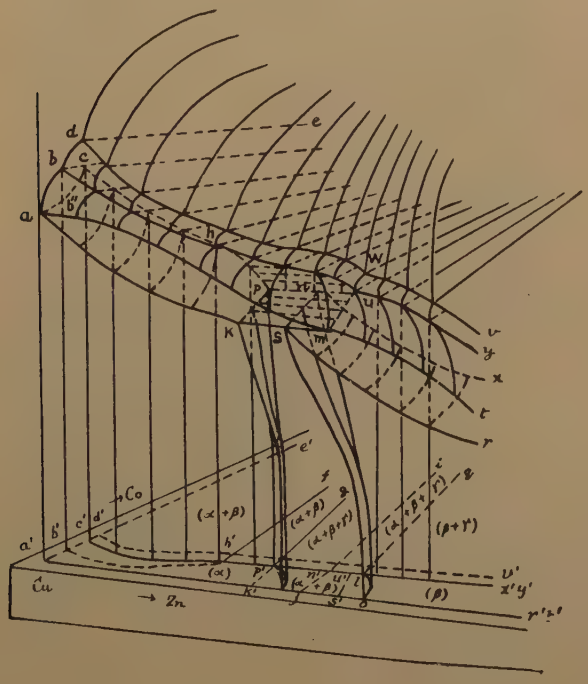

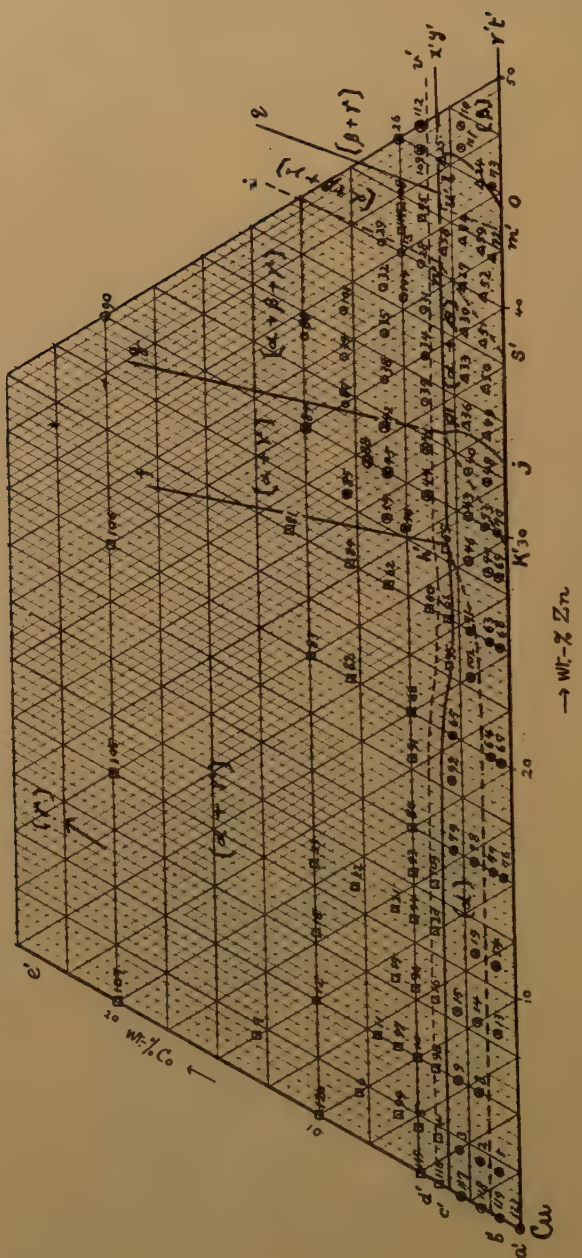

Fig. 6

1 The field–$a'b'h'p'jk'a'$: structure α

The alloys in this field are all of the α-structure at room-temperature, as shown in Photo. I. The melt begins to separate out the α-crystals at the temperatures below those of the liquidus surface and ceases at the temperatures of the solidus-surface enclosing the field $ab''chpka$, where a space-curve pk shows the concentration of the saturated mixed crystals. The boundary-surface, $jkpp'$, which the α-field will form with the seventh field $p'js'm'olu'n'p'$, shows an inclination towards the right when the temperatures are lowered, so that the α-field will get widened at room-temperature in the limit of $p'jk'p'$, which consisted formerly of the bi-structure of α and β.

2 The field–$b'c'h'b'$: structure α

In this field a Co-rich ternary mixed crystal γ begins to separate out of the melt at the temperatures represented by a part of the liquidus-surface $dbhuwd$. The separation continues till the temperatures of the peritectic-surface $bchb$ are reached ; at these temperatures the melt of bh and γ enter on a peritectic reaction on the withdrawal of heat, forming a saturated ternary mixed crystal α represented by a space-curve ch at the expense of all of γ. The melt now in equilibrium with α crystallises entirely at the temperatures of the solidus-surface $ab''chpka$. The structure of this field consists therefore generally of α, but according to the ratio of cooling velocities a skeleton-like structure is sometimes observed due to the peritectic reaction, as shown in Photo. 2.

3 The field–$e'c'h'f$: structure $\alpha+\gamma$

The field concerns the Cu-side, and the Co-side, being saturated, melts immiscibly and in equilibrium at high temperatures. On the fall of temperature, the Co-rich melt begins to separate out the Co-rich ternary mixed crystal γ, when it reaches a space-surface edw, where the composition of the melt becomes so Cu-rich as indicated by the space-curve dw.

At this stage, the Co-rich melt disappears, while the Cu-rich homogeneous melt is left behind. On further cooling, the mixed crystal γ will be separated continuously from the melt till the melt finally takes the composition of the space-curve bh, where it goes on the withdrawal of heat into a peritectic reaction with the mixed crystal γ in order to form α as indicated by a space-curve ch. This reaction comes to end with the disappearance of the melt.

The structure consists therefore of a mixture of α and γ, as may be seen from Photo. 3, where the bright star-like crystals γ are scattered on the ground of α.

4 The field-*fh'p'g*: structure $\alpha+\gamma$

Two immiscible liquids coexist at high temperatures in this field as in the former one. As soon as the temperatures fall to a space-surface *edw*, a Co-rich crystal γ being separated out of the Co-rich melt, the remainder of the liquid becomes by and by Cu-richer, so that it falls finally to the compositions indicated by the space-curve *dw* where the Co-rich liquid disappears.

On cooling further, the melt continues to separate out the Co-rich mixed crystal γ till it reaches the space-curve *hu*. When the temperatures still fall underneath the space-curve *hu*, the Cu-saturated mixed crystal α separates out along the space-curve *hp*, whereupon the melt becoming Cu-less tends to move along the curve *hu* towards the right. In this way, there exists an equilibrium, as represented by a vertical plane *phump*, between the α-crystal along the curve *hp* and the melt along the curve *hu*. Below the temperatures of the curve *hp*, the alloys should all be solid. In so far as elucidated, we may see that the structure of the alloys in this field must also consist of α and γ (Photo. 4), but that the α is of primary nature and not a product of a peritectic reaction as in the third field.

5 The field-*gp'n'i*: structure $\alpha+\beta+\gamma$

One of the two liquids immiscible at high temperatures, namely the Co-rich one, now commences to deposit γ at the temperatures of the space-surface *edw*, as the result of which the liquid tends to become Cu-rich till it acquires at last the compositions of the curve *dw*. On further cooling, it will cause the deposition of the Co-rich crystals along the space-surface *wdbhuw*, and when the temperatures are so low as to touch the space-curve *hu*, the solid phase in equilibrium with the melt will be α along the curve *hp*, while the remainder of the melt will move from *h* to *u* along the curve *hu*. Finally, when the solid phase α stands in equilibrium with the liquid *u*, the withdrawal of heat will result in a peritectic reaction at *n* so as to form a new ternary mixed crystal β.

The structure of the alloys in this field must therefore consist of three phases α, β and γ. (See Photo. 5)

6 *The field–in'u'lq* : structure $\alpha+\beta+\gamma$

On separating γ, the remainder of the melt will finally reach the curve *huy*. A further solidification of the melt must then go on differently either along the curve *hu* (1) or along the curve *uy* (2) :—

1) On being further cooled, the crystal α along the curve *hp* will be separated from the melt *hu* at the same rate as the remainder of the liquid becomes Cu-less. At temperatures so low as the line *pnu*, the Cu-saturated α-crystal (nominated *p*) will enter into a peritectic reaction with the melt *u* so as to give a new solid phase β (nominated *n*). On being lowered temperatures below the space-line *nu*, the composition of β will move along the space-curve *nx* and that of the melt along the space-curve *uy*. At the temperatures of *nx*, all comes to solidify at the expense of the melt.

2) In so much as the crystal β of the space-curve *nx* will be deposited along the decreasing temperatures, the remainder of the melt will change its composition along *uy*, and at the temperatures of the space-curve *nx* all will come to solidify.

As explained, the alloys solidify in both cases to a mixture of β and γ. The structure is, however, changed from the temperatures lower than the space-surface *osnl* by the segregation of α from β, so that the alloys in this field will show a triple structure consisting of α, β and γ at room-temperatures.

7 *The field–p'js'm'olu'n'p'* : structure $\alpha+\beta$

At the temperatures of the liquidus-surface *hum*, the melt separates α as primary crystals, and this will cause the composition on the space-surface *hum* to vary towards the right side, so as to reach the space-line *mu*. Here there takes place a peritectic reaction between α (along the space-line *pk*) and the melt (along the space-line *mu*), as the concequence of which we have β (along the space-line *sn*). The ternary peritectic-surface spreads over as far as shown by the symbol *pksmunp*, and it is the continuity of the binary peritectic-line *ksm* in the Cu–Zn system. Two crystals α and β appear therefore in this field as the structural elements, as shown in Photo. 6.

The reguli having the compositions limited by the liquidus-surface *muh* and the solidus-surface *msnum* separate β only at the temperatures between those of the solidus-surface *rsnx* and of the boundary-surface *osnl*, and beneath the latter all the β segregates α owing to its change in solubility, so that the alloys will show anywhere a binary structure at room-temperatures.

8 The field-*x'lor'* : structure β

The alloys in this field begin to separate β represented by the space-surface *xnsr* at the temperatures of the liquidus-surface *yumt*, the composition of the residual liquid being thereby changed according to the space-surface *yumt*. The solidification is completed at the concave surface *rsnx*. The structure of the alloys is therefore β. (Photo. 7)

The boundary-surface *osnl* runs obliquely downwards and therefore limits the β-field wider at higher temperatures, which is a result following from the fact that β has a greater solubility for α at higher temperatures under the space-surface *rsnx*. For example, the alloy No. 25 (57.01% Cu, 41.43% Zn and 1.56% Co) takes the β-structure on quenching at 800°C (Photo. 8), while it consists of α and β when slowly cooled (Photo. 9). All other details are given in Table XI.

Table XI

No.	Quench. Temp. & Its Structure						
52	900° β	850° α+β	700° α+β	600° α+β	500° α+β		
27	910° α+β	850° α+β	650° α+β	500° α+β			
58	950° α+β+melt	920° α+β	900° α+β	750° α+β	550° α+β		
72	920° α+β+melt	900° β	850° β	800° α+β	750° α+β	600° α+β	500° α+β
59	900° β	850° β	800° α+β	780° α+β	750° α+β	700° α+β	600° α+β
74	900° β	850° β	820° α+β	750° α+β	700° α+β	550° α+β	
24	850° β	820° β	800° β	750° β	700° α+β	600° α+β	550° α+β
25	850° β	800° β	750° β	700° α+β	600° α+β	550° α+β	
73	800° β	700° β	600° β	500° β			
111	850° β	800° β	700° β	640° β	550° β		

9 The field-*qlx'* : structure $\beta+\gamma$

Depositing γ at falling temperatures, the Co-side liquid in equilibrium changes its composition till it reaches at last the space-curve *vv*, where the equilibrium comes to end. Down from these temperatures, the residual liquid still continues to give out γ along the liquidus-surface *vwuy* till it reaches finally the space-curve *uy*. Hereupon, the melt begins, on the withdrawal of heat, to deposit β (along the space-curve *nx*) vertically down

along the space-plane *xnuy*. The solidification now concludes at the space-curve *nx*.

The structure of the alloys consists therefore of β and γ. (Photo. 10)

Sectional Diagrams of the Equilibrium-Model

Five sectional diagrams were obtained by cutting the equilibrium-model with vertical planes, OP, QR, ST, VW and XY as shown in Fig. 7. These are given in Fig. 8–12.

Fig. 7

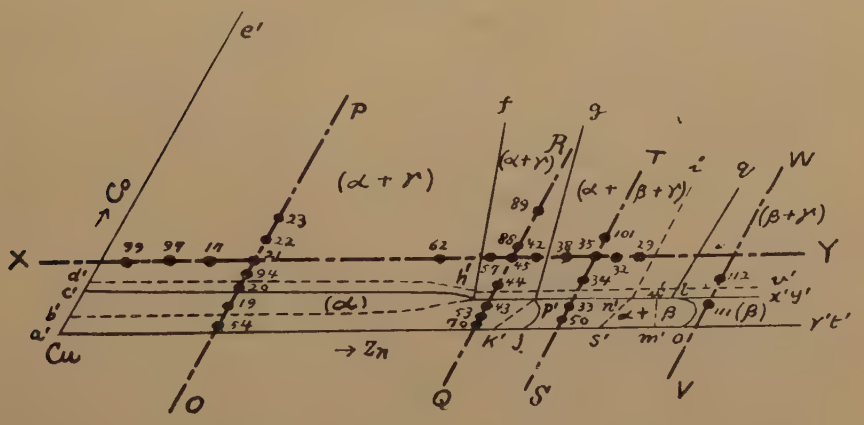

Fig. 8

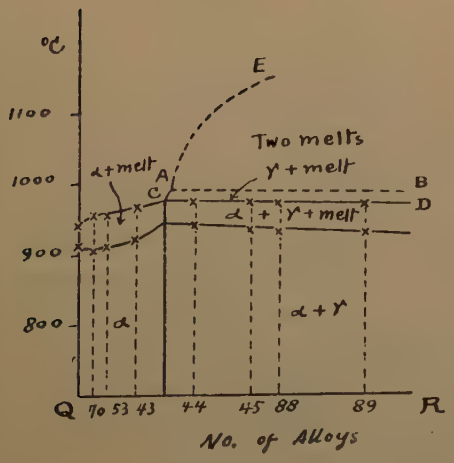

Fig. 9

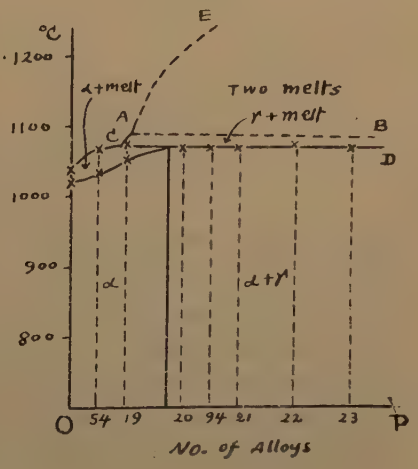

Fig. 10

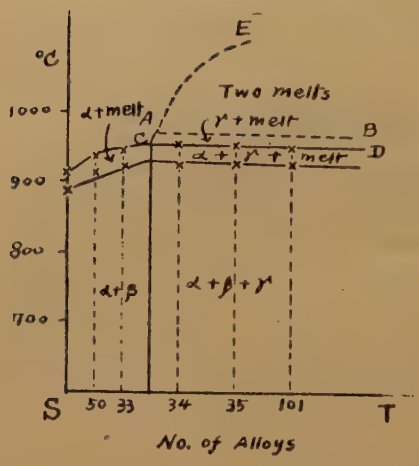

Fig. 11

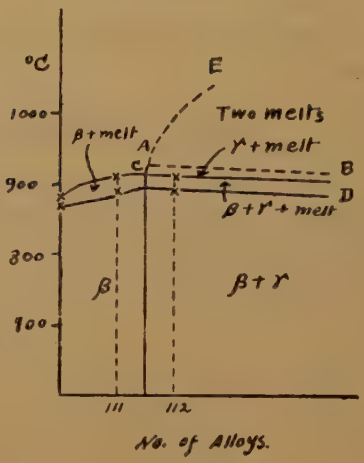

Fig. 12

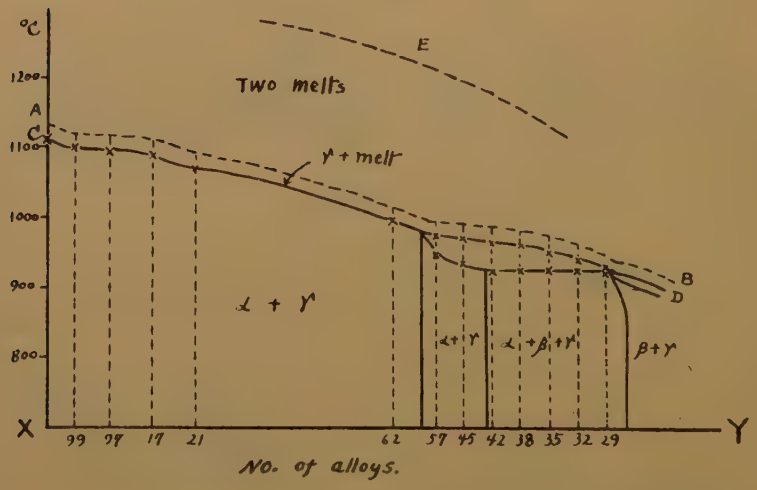

The dotted line AE shows a part of the conjugate line representing the equilibrium-state between the two immiscible liquids. Their temperatures of equilibrium are not to be measured.

The dotted horizontal line AB indicates the beginning temperatures of primary crystallisation of γ in the Co-rich melt.

No thermal effect due to γ is clearly to be perceived, because the Co-content is too small in the limits of our determination.

Mechanical Tests

Test bars of definite compositions, cast in sand moulds, were machined down to the required dimensions, as shown in Fig. 13. After annealing for one hour, in order to secure uniformity in composition, they were subjected to tests for ultimate strengths and elongation percentages. The results are given in Table XII.

Fig. 13

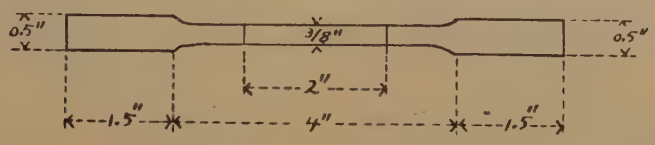

Table XII

Mark	Composition—%			Ultimate Strength Tons per sq. in.	Elongation Per Cent on 2 in.
	Cu	Zn	Co (diff.)		
A	60.82	39.04	—	4.09	25.00
E	59.47	39.44	1.09	4.15	28.13
B	59.79	38.08	2.13	4.41	28.13
C	59.61	37.29	3.10	4.20	25.00
D	59.02	37.07	3.91	3.64	18.75
F	70.50	29.69	—	2.89	43.75
I	71.85	27.01	1.14	3.01	34.37
G	72.07	26.08	1.85	3.25	31.25
H	70.87	26.39	2.74	2.92	13.12

Addition of 1%–2% of Co raises the tensile strength of the F-alloy (70 : 30-brass) at the expense of a slight amount of elongation, and both the strength and the elongation of the A-alloy (60 : 40-brass).

These facts lead us to the generalisation, that β-brass is improved in all its mechanical properties by addition of Co, while α-brass is improved in strength but not in elongation. Reference shonld be made to Table XII, alloys I, G and H. We see, therefore, that A-alloy, on the addition of Co,

will gain much more elongation in α than it will lose in β, which results in the improvement of its properties as a whole. Alloys E and B, Table XII, are examples of improved brasses.

Corrosion Tests

A series of experiments was carried out for corrosion in sea-water with several Co-containing 60 : 40-brasses, the compositions of which are given in Table XII.

These alloys were immersed in artificial sea-water with 5% NaCl by weight, which was kept nearly constant at 100°C in a water-bath. After 50 and 100 days, they were taken out of the sea-water, scrubbed carefully with a brush, washed with hot water, dried at 200°C and then weighed. Losses in weight were recalculated for grams per 5 cm^2.

The details of the researches are given in Table XIII, and their purport is this :—

60 : 40-brass with 3%–4% Co added is more resistant against sea-water than simple brass. The compositions of the best alloys are marked C and D in the Table.[1]

Table XIII

Mark	Surface area of alloy $cm.^2$	Original Wt. of alloy gr.	Wt. after 50 days gr.	Wt. after 100 days gr.	Final loss in Wt. gr.	Loss in Wt. per 5 $cm.^2$ gr.
A	3.77	5.8120	5.7712	5.7450	0.0676	0.0888
E	3.77	5.2013	5.1687	5.1500	0.0513	0.0680
B	2.76	3.2943	3.2759	3.2647	0.0296	0.0536
C	2.43	2.7550	2.7457	2.7368	0.0182	0.0374
D	2.97	2.8265	2.8180	2.8113	0.0152	0.0256
T	2.76	3.3058	3.2863	3.2728	0.0330	0.0598
Y	3.25	2.9080	2.8820	2.8725	0.0355	0.0546

In conclusion, the author wishes to acknowledge his indebtedness to Prof. M. Chikashige for his valuable suggestions throughout the course of the investigation.

1 Naval brass, Y- and T-alloys, does not show any superiority over our cobalt-brass as co-tabulated in the Table.

Y-alloy: 59.07% Cu, 38.88% Zn, 2.05% Sn.
T-alloy: 59.61% Cu, 39.42% Zn, 0.97% Sn.

Plate I

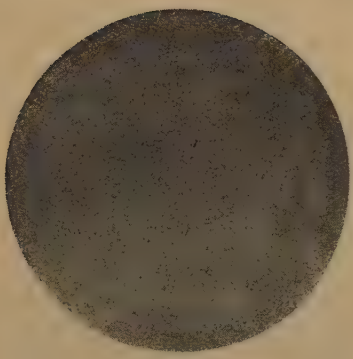

Photo. 1. No. 68–alloy.
Cu 74.89%, Zn 24.61%, Co 0.50%.
As Csat. ×120.

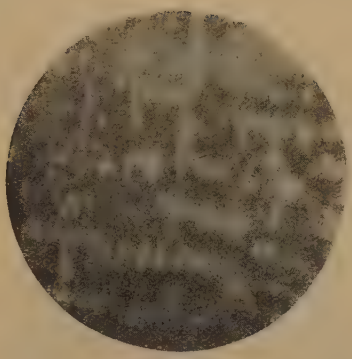

Photo. 2. No. 71–alloy.
Cu 74.03%, Zn 24.39%, Co 1.58%.
As Cast. ×120.

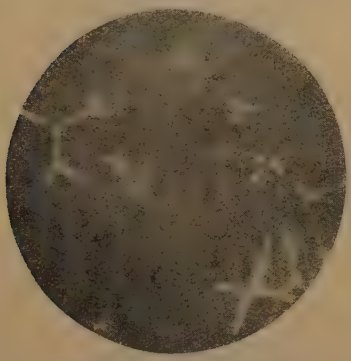

Photo. 3. No. 61–alloy.
Cu 72.18%, Zn 24.88%, Co 2.94%.
As Cast. ×120.

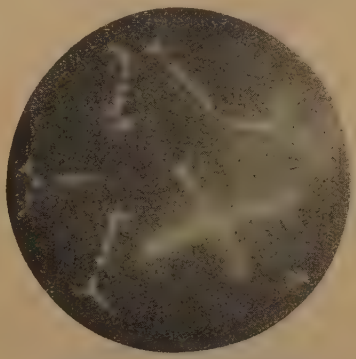

Photo. 4. No. 88–alloy.
Cu 63.72%, Zn 29.18%, Co 7.10%.
As Cast. ×120.

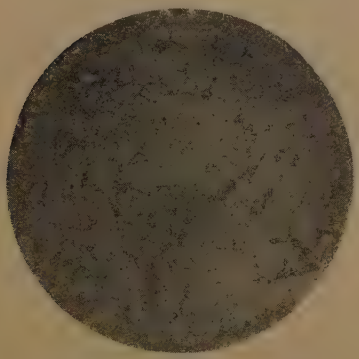

Photo 5. No. 101–allor.
Cu 57.08%, Zn 35.72%, Co 7.20%.
As Cast. ×120.

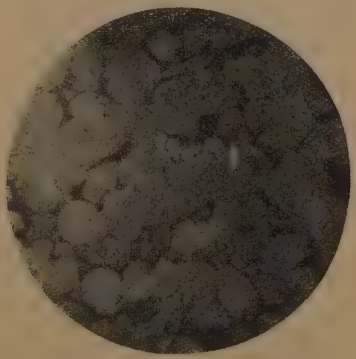

Photo. 6. No. 33–alloy.
Cu 62.12%, Zn 35.69%, Co 2.19%.
As Cast. ×120.

Plate II

Photo. 7. No. 111-alloy.
Cu 51.84%, Zn 45.69%, Co 2.47%.
As Cast. ×120.

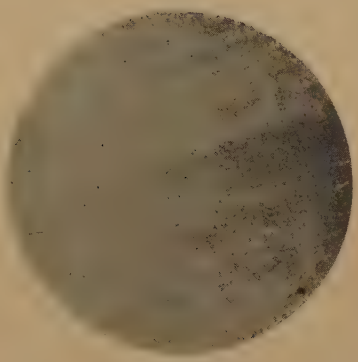

Photo. 8. No. 25-alloy.
Cu 57.01%, Zn 41.43%, Co 1.56%.
Quench. at 809°C. ×120.

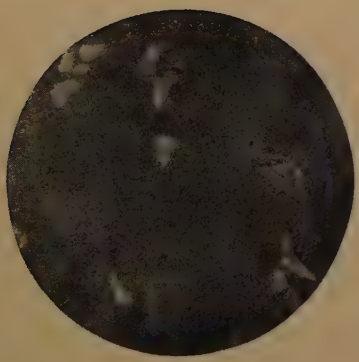

Photo. 9. No. 25-alloy.
(The same as Photo. 8)
As Cast. ×120.

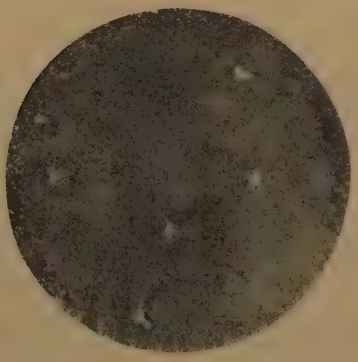

Photo. 10. No. 26-alloy.
Cu 51.21%, Zn 44.88%, Co 3.91%.
As Cast. ×120.

An Examination of the Micro-Crystals of Calcium Carbonate in Molluscan Shells by Means of X-Rays, Part III

By

Jinzo Tsutsumi

(Received May 6, 1929)

Abstract

Testing the shells of more than 60 species of Japanese Molluscs by means of the X-ray method, it is proved that there exist various degrees of fibrous arrangement of the micro crystals of calcium carbonate in the molluscan shells. In all of them the axes of the fibrous arrangement are in a direction nearly perpendicular to the surface of the shell, coinciding with the principal axis of calcite or with the orthorhombic *c* axis of aragonite respectively.

The form and arrangement of the micro-crystals of calcium carbonate in *Atrina*, *Avicula*, *etc.* were examined by Ebner, Biedermann and others[1] nearly thirty years ago with the microscope or by passing a plainly polarized light through the shells. Such optical methods, however, are only available in a few kinds of shells which are composed of sufficiently large micro-crystals of calcium carbonate. For the majority of the shells they are inefficient for that purpose, whereas, the X-ray method involves no such restriction, and is good for any kinds of shells. As was stated in his previous papers[2], the writer utilized the monochromatic X-rays from the

1. Biedermann, W.; Ztschr. f. all. Physiol., Bd. **1**, (1902)
   „ „ ; Jena Ztschr., Bd. **36**, (1901)
   „ „ ; Biol. Ctbl., Bd, **21**, (1901)
   Ebner, V. ; Sitz.-ber. d.Wiener Akad., math.-nat. Kl., Abt. 2, Bd. **89**, (1884–85) & Bd. **91**, (1885)
   Dippel, L. ; Zeitschr. f. Wiss. Mikrosk. Bd. **17**, (1900)
2. J. Tsutusmi ; These Memoirs, A, **11**, 217 & 401 (1928)

Mo-target in the examination of the micro-crystals of calcium carbonate in the shell of *Atrina japonica* Reeve, and was able to determine their crystal-forms as well as their arrangement very easily. The same method was applied now to examine various shell specimens of more than 60 different species of Molluscs. The results thus obtained are as described below.

A diagram of the X-ray diffraction patterns obtained with the prismatic and the nacreous layers respectively of the shell of *Atrina japonica* Reeve, by a parallel incidence of the X-rays to the surface of the layer, are shown here again in Text-figs. 1 and 2. Fig. 1[1] illustrates the

Fig. 1

The prismatic layer

Fig. 2

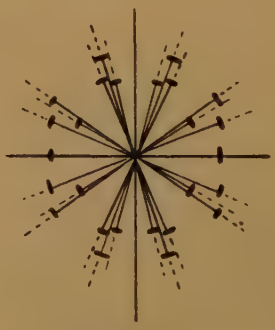

The nacreous layer

X-ray diffraction pattern of the prismatic layer, most parts of which are composed of micro-crystals of calcite, while Fig. 2[2] shows that of the nacreous layer, most parts of which are composed of micro-crystals of aragonite. The revelation of the diffraction patterns as shown in these figures indicates that the micro-crystals of calcium carbonate in both these layers are arranged fibrously, and also that the axis of such fibrous arrangement is nearly parallel to a direction perpendicular to the surface of the layer coinciding with the principal axis of calcite or the orthorhombic *c* axis of aragonite respectively.

First the diffraction photographs with X-rays were taken of about 10 different shells belonging to the order of Lamellibranchia, by sending the X-rays in a direction parallel to the surface of the layer of the shells, and some of them have been reproduced in Plate I, Figs. 1, 2, 3 and 4 as

1. J. Tsutsumi ; These Memoirs, A, **11**, 217 (1928) & H. Fukushima ; „ „ A, **11**, 223 (1928)
2. J. Tsutsumi ; „ „ A, **11**, 401 (1928)

typical ones. Figs. 1 and 2 in Plate I are diffraction figures obtained with a shell of *Mytilus crassitesta* Lischke. This shell consists of two layers, each of which is stratiform. In the outer layer of the shell the calcium carbonate is in the form of calcite, while that in the inner layer is in the form of aragonite. By comparing these photographs with the foregoing Text-figs. 1 and 2, we see that the micro-crystals of calcium carbonate in the shell are arranged fibrously in the direction nearly perpendicular to the surfaces of the layers, and that the principal axis of calcite as well as the orthorhombic *c* axis of aragonite are arranged as the axis of the fibre, as was the case in the prismatic or in the nacreous layers of *Atrina japonica* Reeve. The diffraction patterns obtained with *Anomia lischkei* Dautzenberg et Fischer and *Pinctada martensi* Dunker, which also belong to the order of Lamellibranchia, are reproduced in Plate I, Figs. 3 and 4. The distribution of radiating bands and the dispersal of intense spots on these bands perceived in these photographs are essentially the same as in Figs. 1 and 2 in Plate I respectively. This fact indicates that the crystal-forms and the arrangement of the micro-crystals of calcium carbonate in the shell of *Anomia* and *Pinctada* are identical respectively with those of the micro-crystals in the prismatic and in the nacreous layers of the shell of *Atrina japonica* Reeve. Next the writer examined the shell of 8 more different species in the same order and was able to ascertain that the crystal-forms and the arrangement in question are the same as those in the nacreous layer of *Atrina japonica* Reeve. Then the writer tried different shells of ca. 30 species of Eulamellibranchia, 4 species of Aspidobranchia, 6 species of Pectimibranchia, 2 species of Streptoneura, 1 species of Placophora, and 1 species of Dibranchia. The diffraction patterns obtained with the shells of *Sunetta excavata* Hanley, *Gomphina melanaegis* Roemer, *Turbo cornutus* Solander, *Fusinus perplexus* A. Adams, *Haliotis asinina* Linne, *Cardium muticum* Reeve, *Dentalium hexagonum* Gould are shown, as typical ones, in Figs. 5, 6, 7, 8, 9, 10 and 11 of Plates I and II. All these photographs were taken by setting the surface layer of the shells parallel to the X-ray beam. The results thus obtained with most of the shells are again essentially the same as in the case of the nacreous layer of *Atrina japonica* Reeve. There are, however, some exceptional cases; in *Fusinus perplexus* A. Adams, *Dentalium hexagonum* Gould, most of the micro-crystals are not arraged fibrously. Moreover in *Cardium muticum* Reeve the micro-crystals are arranged quite irregularly as seen in Plate II, Fig. 10, which is a photograph taken by setting the shell of *Cardium* in various orientations; i. e. to be exposed to the incident X- ray beam.

Up to now the writer has examined the shells of more than 60 different species belonging to various orders, arriving at the following general conclusion. Calcium carbonate in the porcelaneous and the nacreous layer of the molluscan shells is in the form of aragonite while that in the prismatic layer of them is usually in the form of calcite, but in a few cases in the form of aragonite. As to the constitution of the micro-crystals of calcium carbonate, there are various degrees of the fibrous arrangement, but the axis of the fibrous arrangement is always in a direction nearly perpendicular to the outer surface of the shell, and coincides with the principal axis of calcite or the orthorhombic *c* axis of aragonite respectively. So far as the writer's experiment goes, it seems that the more perfect the appearance of the strata, the more perfect the fibrous arrangement of the micro-crystals of calcium carbonate. Since the shell materials for this test was so selected as to cover as evenly as possible all orders of Molluscs, it seems to the writer reasonable that the general conclusions stated above are also good for the other shells not yet examined.

This study was carried out under the supervision of Prof. T. Kawamura and Prof. U. Yoshida, to whom the writer's sincere thanks are here expressed. He is also indebted to Mr. T. Kuroda who was so kind as to assist him in the present investigation.

Plate I

Fig.1

The outer layer of
Mytilus crassitesta Lischke

Fig.2

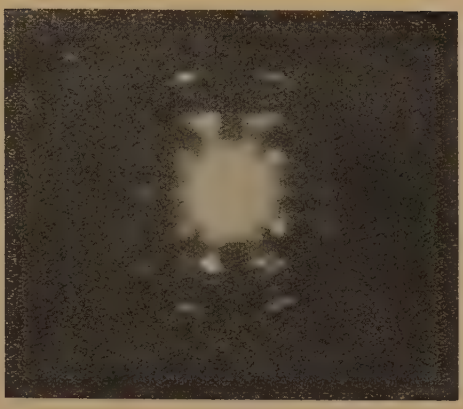

The inner layer of
Mytilus crassitesta Lischke

Fig.3

Anomia lischkei
Dautzenberg et Fischer

Fig.4

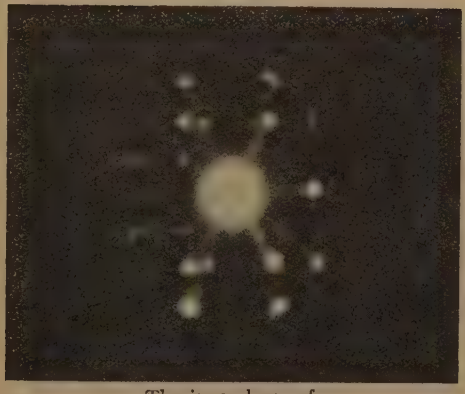

The inner layer of
Pinctada martensi Dunker

Fig.5

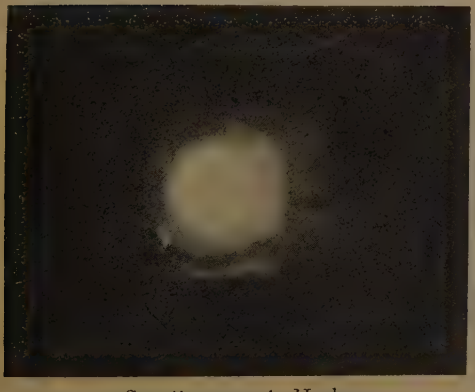

Sunetta excavata Hanley

Fig.6

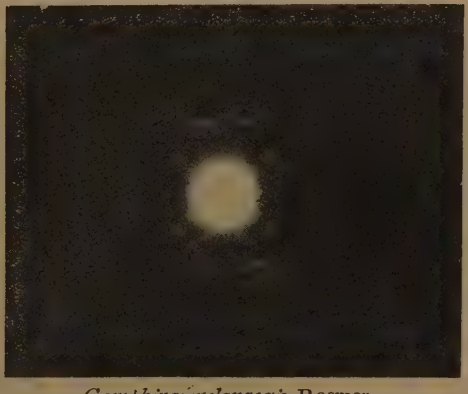

Gomphina melanaegis Roemer

Plate II

Fig.7

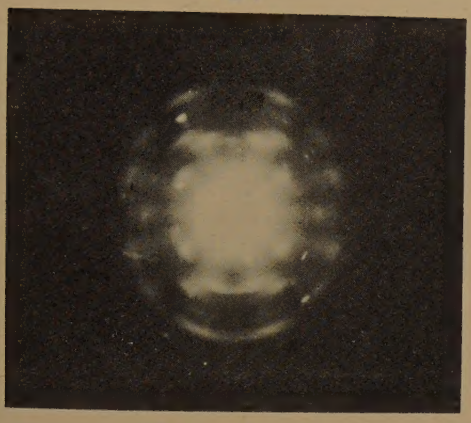

The inner layer of
Turubo cornutus Solander

Fig.8

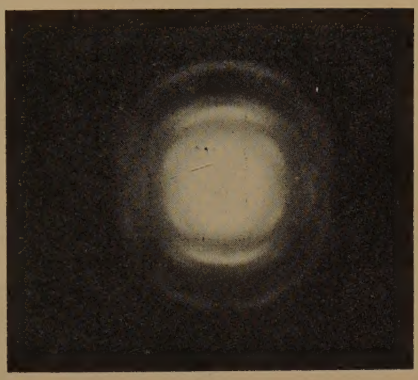

Fusinus perplexus A. Adams

Fig.9

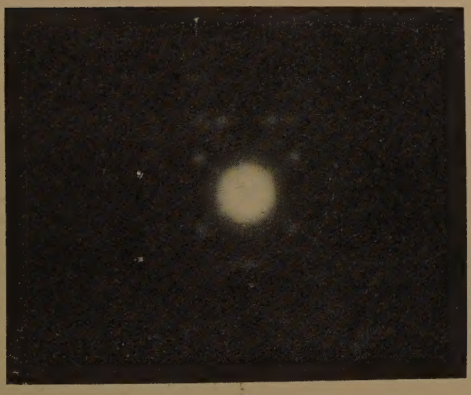

Haliotis asinina Linne

Fig.10

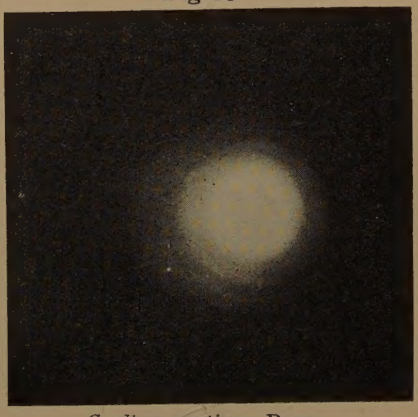

Cardium muticum Reeve

Fig.11

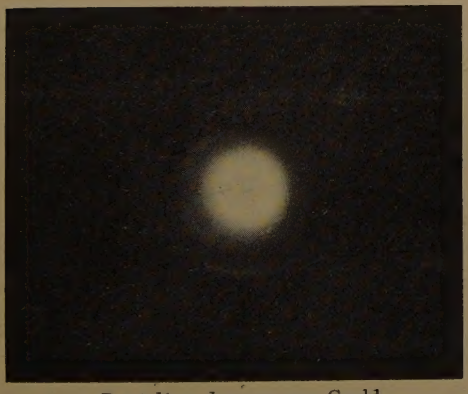

Dentalium hexagonum Gould

Vol. XII, No. 3, Published May 30, 1929

Price - - - Yen 1.300

These Memoirs are on Sale at

MARUZEN COMPANY, LTD.

TOKYO, OSAKA, KYOTO, NAGOYA, YOKOHAMA, FUKUOKA
& SENDAI

昭和四年五月二十五日印刷
昭和四年五月三十日發行

編纂兼發行者　京都帝國大學理學部

印刷者　須磨勘兵衛
京都市下京區北小路通新町西入

印刷所　內外出版印刷株式會社
京都市下京區西洞院七條南

賣捌所　丸善株式會社
東京、大阪、京都、名古屋、横濱、福岡、仙臺

CONTENTS

A Sensitive Reaction of Cuprous Ion
By Otozo Funakoshi 155

Crystal-Faces developed by etching Metallic Crystals of Aluminium and Zinc
By Buntaro Fujita 159

Tensile Strength and Fracture of Rolled Strips of Molybdenum
By Takeo Fujiwara 165

On the Effect of mixing Small Quantities of Cobalt with Brass
By Daidzi Iitsuka 179

An Examination of the Micro-Crystals of Calcium Carbonate in Molluscan Shells by Means of X-Rays, Part III
By Jinzo Tsutsumi 199